Japanese Journal of Applied Physics

The Japan Society of Applied Physics

REGULAR PAPER

Measurement of propagation of local and minute contractile response in layered myocardium

Japanese Journal of Applied Physics **60**, SDDE02 (2021) **REGULAR PAPER**
https://doi.org/**10.35848/1347-4065/abeabf**

Measurement of propagation of local and minute contractile response in layered myocardium

Yu Obara[1], Shohei Mori[2*], Mototaka Arakawa[1,2], and Hiroshi Kanai[2,1]

[1]*Graduate School of Biomedical Engineering, Tohoku University, Sendai 980-8579, Japan*
[2]*Graduate School of Engineering, Tohoku University, Sendai 980-8579, Japan*

[*]E-mail: mori@ecei.tohoku.ac.jp

Received November 30, 2020; revised January 19, 2021; accepted March 1, 2021; published online March 25, 2021

The in vivo measurement of the contractile response caused by electrical excitation has been studied to detect myocardial ischemia in its early stages. In the present study, we used our previously proposed local velocity estimator to measure the two-dimensional distribution of the strain rate using high-density beam scanning to obtain propagation of the local and minute contractile response in the heart walls of healthy humans. Alternate layers of contraction and relaxation were observed around the time phase representing the onset of the conduction of electrical excitation. The contraction propagated along the direction of the myocardial fiber in the myocardial layer. These results indicated that the electrical excitation conducted in each myocardial layer and the transmural shearing deformation occurred at the boundary between alternate layers of contraction and relaxation. The measurement of the propagation of the local and minute contractile response can reveal the effective contraction with the transmural shearing deformation. © 2021 The Japan Society of Applied Physics

1. Introduction

The early detection of myocardial ischemia helps prevent the onset of fatal ischemic events, such as myocardial infarction. Myocardial ischemia occurs in the endocardial region of the heart wall and progresses transmurally toward the epicardial region.[1–3] Thus, local measurement in the transmural direction of the heart wall has the potential to detect myocardial ischemia in its very early stages and assess the progression of myocardial infarction.

Ultrasound diagnosis has the potential to detect diastolic and systolic dysfunction in the early stage of ischemic cascade.[4,5] Ultrasound-based measurements of myocardial strain and strain rate (SR) have been developed to evaluate regional myocardial function.[6–11] The myocardial strain and SR, obtained by removing the whole motion of the heart wall, represent the change in the myocardial thickness. Previous studies have indicated the possibility of identifying myocardial ischemia[12–14] or myocardial infarction[15–17] using myocardial strain and SR as well as the importance of the transmural locality of the strain and SR measurements.[18–20] The improvement of the locality of the strain and SR measurements may help reveal contractions in the layered myocardium and clinical application for ischemic heart diseases.

Myocardial contractile response, caused by electrical excitation, has been studied to detect myocardial ischemia in its early stages. It is well known that the conduction of electrical excitation in the heart wall activates the myocardial contractile response[21] and causes complex dynamics. The propagation of the myocardial contractile response has been confirmed by measuring the myocardial velocity,[22–25] displacement,[26,27] strain,[28,29] and SR[30] around the time phase representing the onset of the conduction of electrical excitation. It has been suggested that myocardial ischemia causes an abnormal propagation of the myocardial contractile response.[23,28,29]

However, the propagation established by measuring the displacement or strain waveforms, obtained by integrating the velocity or SR waveforms, might contain not only the myocardial contractile response caused by electrical excitation but also other components because several natural mechanical waves propagate in the heart wall during this short time phase.[22,31,32] The changes caused by large natural mechanical waves in the displacement or strain waveform may be dominant than those caused by the minute myocardial contractile response. Moreover, the myocardial velocity and displacement contain the whole motion of the heart wall; however, the myocardial strain and SR do not contain them. Thus, myocardial SRs in the heart wall can capture the propagation of the myocardial contractile response in detail.

As the myocardial SRs are calculated using the velocities obtained at multiple positions in the heart wall, local velocity estimation is essential for the local measurement of SR. In previous studies,[7,30,33–35] the transmural SR distribution was measured at different depths in the heart wall with high temporal resolution using the phased-tracking method.[36] However, it has been difficult for the conventional velocity estimator[36] to measure the minute changes in the spatially local myocardial thickness because the estimated velocity is averaged spatially by the cross-correlation function. We proposed the multifrequency phased-tracking method to improve the locality of the velocity estimation.[37] Using the proposed local velocity estimator,[37] minute changes in the spatially local myocardial thickness have been measured, which exhibit alternate layers of contraction and relaxation.[38]

Two-dimensional distribution of myocardial SR, with high-density beam scans, is required to obtain the propagation of the minute changes in the local myocardial thickness. The two-dimensional SR distribution was measured to visualize the propagation of the contraction and relaxation in the heart wall.[30] In this study, low-density (sparse) beam scanning[24,30] was applied to locally measure the SR to realize a high-frame-rate measurement using a focused wave. Additionally, a conventional velocity estimator with an averaging operation in the depth direction was used. However, the low-density beam scans and the low-locality SR measurement challenged the detailed measurement of the propagation of the minute change in the local myocardial thickness in the lateral direction.

In the present study, we measured the two-dimensional distribution of the myocardial SR with high-density beam scans, using the multifrequency phased-tracking method. The propagation of the minute change in the spatially local myocardial thickness was observed in the two-dimensional

distribution of the myocardial SR, around the time phase representing the onset of the conduction of electrical excitation, to reveal the mechanism of the effective contraction of the heart. We discuss the measured propagation of the local and minute contractile response in the SR distribution from the perspective of the physiological mechanism of the heart.

2. Methods

2.1. Ultrasonic measurement with high-density beam scans and high frame rate

Figure 1(a) shows the schematics of the low-density beam scans used in the previous study[30] and high-density beam scans in the present study. To increase the density of the ultrasound beam scans in the lateral direction compared with that of the previous study,[30] the spatial interval of the ultrasound beams was set at 1.5°, wherein the density of the ultrasound beam scans was more than three times higher than that of the previous study (5.6°).

Measurement using a focused wave has a higher spatial resolution than a plane wave or a diverging wave. Thus, the acquisition area of the radiofrequency (RF) signals was limited to realize a dense measurement with a high frame rate using a focused wave. The viewing angle of the acquisition area was reduced to 24°, compared with 45° used in the previous study. In the measurements, the frame rate, f_{FR}, of the acquisition of the RF signals was set at 503 Hz, which was 630 Hz in the previous study.[30]

2.2. Measurement environment

In vivo measurements were applied to three healthy subjects in their twenties using an ultrasound diagnostic apparatus. The measurements were approved by the Ethics Committee of Tohoku University. Additionally, all subjects agreed to participate in this study.

A focused wave was transmitted from a sector probe (UST-52105; Hitachi-Aloka-Medical Ltd., Tokyo, Japan) connected to an ultrasound diagnostic apparatus (F75; Hitachi-Aloka-Medical Ltd., Tokyo, Japan). The center frequency of the transmitted wave was 3 MHz, and the sampling frequency f_s was 20 MHz. Assuming that the speed of sound of the tissue, c_0, is 1540 m s^{-1}, the spatial interval of the sampling points in the ultrasound beam direction is 0.038 mm. Electrocardiogram (ECG) and phonocardiogram (PCG) waveforms were acquired simultaneously in the measurements. For each subject, the ECG waveform was measured for lead II using the three-point lead method, and the PCG waveform was measured using a microphone attached to the subject's chest.

Figures 1(b) and 1(c) show the schematic of the in vivo measurement and the B-mode image of the cross-section in the parasternal long-axis view, respectively. The acquisition area of the RF signals was limited to the interventricular septum (IVS) to realize a high-frame-rate measurement. In the parasternal long-axis view, the mitral valve (MV) was used as a landmark such that the right-side boundary of the

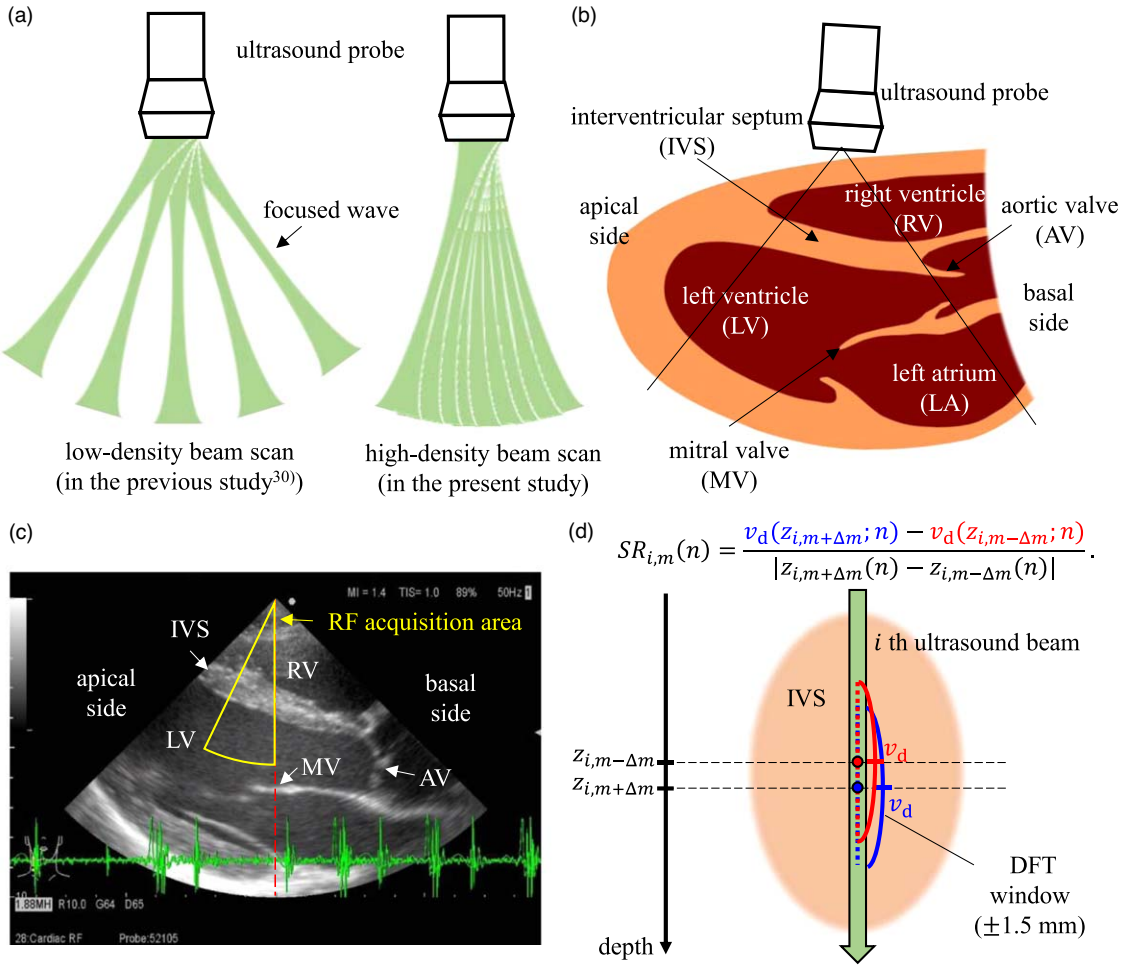

Fig. 1. (Color online) (a) Schematics of low-density beam scans and high-density beam scans. (b) Schematic of in vivo measurement. (c) B-mode image of the cross-section in parasternal long-axis view. (d) Schematic of calculating strain rate (SR).

acquisition area was set by the ultrasound beam located above the MV, as shown in Fig. 1(c).

2.3. Local velocity estimation using multifrequency phase differences[37)]

In the present study, the local velocity in the ultrasound beam direction was estimated at multiple positions in the heart wall using the multifrequency phased-tracking method.[37)] The process of local velocity estimation, presented as follows, was based on that described by referring to Ref. 37.

The RF signal of the ith ultrasound beam in the nth frame, $s_i(t, n)$, was cut out around the mth position using a Hanning window (±1.50 mm). The frequency spectrum $S_{i,m}(f, n)$ was obtained by applying discrete Fourier transform (DFT) to the windowed signal, $s_{i,m}(t, n)$. In the $(n + 1)$th frame, the frequency spectrum, $S_{i,m}(f, n + 1)$, was also obtained by employing the same procedure. The cross-spectrum between consecutive frames, $C_{i,m}(f, n)$, was calculated as

$$C_{i,m}(f, n) = S^*_{i,m}(f, n) \cdot S_{i,m}(f, n + 1), \tag{1}$$

where * denotes the complex conjugate.

The phase gradient, $a_{i,m}(n)$, of the cross-spectrum was estimated by the least-square method using the amplitude of the cross-spectrum, $|C_{i,m}(f, n)|$, as a weighting function. Assuming that the velocities in the window of the DFT are uniform between consecutive frames, the estimated velocity, $\hat{v}_d$, between consecutive frames can be expressed using the estimated phase gradient, $\hat{a}_{i,m}(n)$, of the cross-spectrum as follows:

$$\hat{v}_d(z_{i,m}; n) = \frac{c_0 f_{FR}}{4\pi} \cdot \hat{a}_{i,m}(n). \tag{2}$$

Here, $z_{i,m}$ is the depth of the mth position in the ith beam and c_0 is the speed of sound of the living tissue.

As the phase gradient of the cross-spectrum is estimated using the multifrequency phase differences, the influence of the frequency-dependent attenuation and interference of backscattered waves can be suppressed.[37)] Thus, velocity can be estimated locally without the spatial averaging operation caused by the calculation of the cross-correlation function.

2.4. Measurement of SR distribution in the heart wall

The myocardial SR distribution was calculated from the velocities obtained at multiple positions in the heart wall. As shown in Fig. 1(d), the SR on the mth position in the ith beam was calculated as[31,35,36)]

$$SR_{i,m}(n) = \frac{v_d(z_{i,m+\Delta m}; n) - v_d(z_{i,m-\Delta m}; n)}{|z_{i,m+\Delta m}(n) - z_{i,m-\Delta m}(n)|}, \tag{3}$$

where Δm is the interval of the sampling points used to calculate the SR. In the present study, the initial interval $|z_{i,m+\Delta m}(0) - z_{i,m-\Delta m}(0)|$ was set to 0.821 mm. The interval in the nth frame, $|z_{i,m+\Delta m}(n) - z_{i,m-\Delta m}(n)|$, was determined by tracking the $(m + \Delta m)$th and $(m - \Delta m)$th positions, respectively, by integrating the velocity waveform. The SRs were obtained at several hundred positions in the depth direction in each ultrasound beam, using which the two-dimensional distribution of the SR was obtained.

In the parasternal long-axis view, it is assumed that the ultrasound beam is perpendicular to the myocardial fiber direction in each myocardial layer. As the myocardial thickness increases (decreases) when the myocardium contracts (relaxes) in the fiber direction, the positive (negative) SRs indicate myocardial contraction (relaxation).

3. Results

3.1. Two-dimensional distribution of myocardial SR using local velocity estimator

Figure 2 shows the two-dimensional distribution of the myocardial velocity and SR of the IVS at several time phases

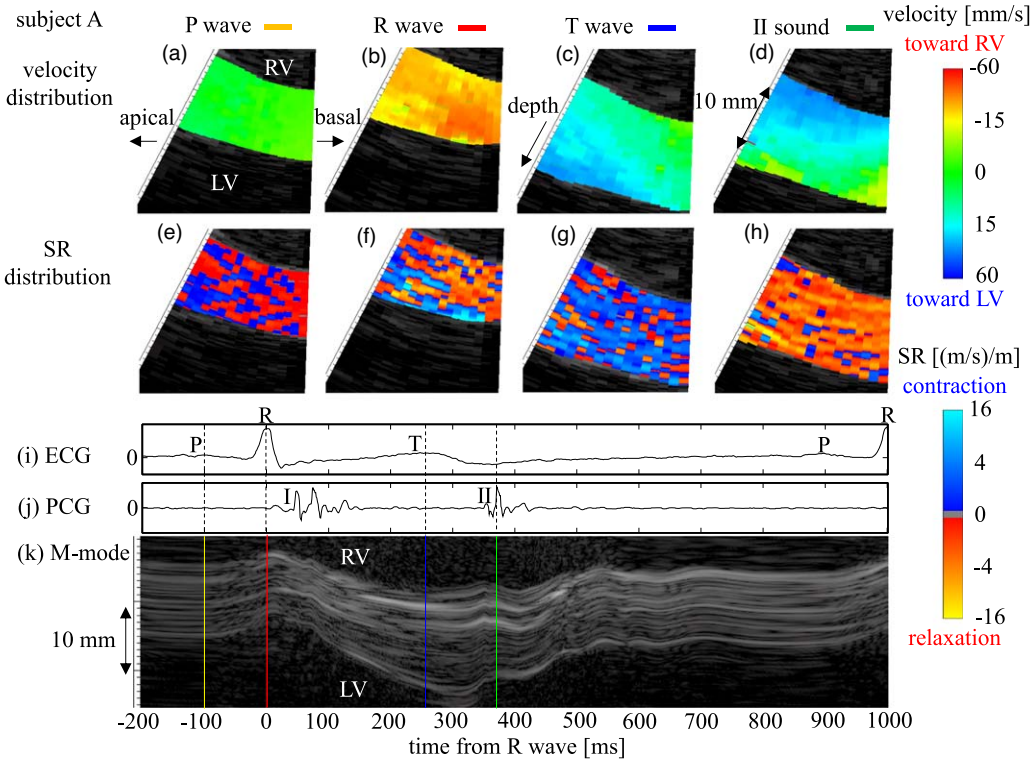

Fig. 2. (Color online) (a)–(d) Two-dimensional distributions of velocity of the ultrasound beam and (e)–(h) two-dimensional distributions of SR at several time phases in a cardiac cycle. (i) Electrocardiogram (ECG) waveform. (j) Phonocardiogram (PCG) waveform. (k) M-mode image in the central beam.

in a cardiac cycle. The blue and red colors in the velocity distribution represent the velocity toward the left ventricular (LV) and right ventricular (RV), respectively. In the SR distribution, the cold and warm colors represent the myocardial contraction and relaxation, respectively. At the time of the ECG P-wave, the values of the SR in the IVS were approximately zero; i.e. the myocardia in the IVS did not contract. However, at the time of the ECG R-wave, the SR distribution shows alternate layers of contraction and relaxation, especially on the apical side. However, the velocity distribution does not show the layers, as shown in Fig. 2(b).

In a previous study using the multifrequency phased-tracking method,[38] the alternate layers of contraction and relaxation were observed clearly in each ultrasound beam. In the present study, similar alternate layers of contraction and relaxation were confirmed in each ultrasound beam. Moreover, the alternate layers were measured as spatially continuous in the longitudinal direction of LV, as shown in Fig. 2(f), although the myocardial SRs were calculated independently for each ultrasound beam. This continuity of SR distribution in the longitudinal direction indicated that the alternate layers of contraction and relaxation reflect the physiological mechanism of the heart.

Figure 3 shows the SR distribution at the time of the ECG R-wave in three consecutive heartbeats for three subjects. The alternate layers of contraction and relaxation, continuous in the longitudinal direction, were observed for all the subjects and their heartbeats.

3.2. Propagation of local and minute myocardial contractile response

The two-dimensional distributions of SR were measured around the time phase of the ECG R-wave. Figure 4 shows the two-dimensional SR distributions every 2 ms for subject A around the time phase of the ECG R-wave. At −14 ms from the ECG R-wave, a rapid contraction (cold color) of the myocardium was observed in several myocardial layers on the apical side of the LV side of the IVS, as shown in Fig. 4(a). Then, the rapid contraction propagated from the apical side to the basal side in the longitudinal direction until the time of the ECG R-wave and the contractile region gradually increased after the ECG R-wave. Although the same SR pattern was not obtained even for three consecutive heartbeats for the same subject, the propagation of the rapid contraction from the apical side to the basal side followed the same pattern.

Figures 5 and 6 show the two-dimensional distributions of the myocardial SR around the time phase of the ECG R-wave every 2 ms for subjects B and C, respectively. As shown in Figs. 5 and 6, the rapid contraction on the LV side of the IVS propagated from the apical side to the basal side for subjects B and C, similar to that observed in subject A. Especially on the LV side of the IVS, the propagation of the rapid contraction in the longitudinal direction was confirmed for all subjects.

4. Discussion

4.1. Usefulness of local and dense measurement of two-dimensional distribution of myocardial SR

In a previous study that used the multifrequency phased-tracking method,[38] the alternate layers of contraction and relaxation were confirmed in each ultrasound beam around the time phase representing the onset of the conduction of electrical excitation. However, the relationship between the alternate layers and the physiological mechanism of the heart were not discussed because of the low-density beam scans. In the present study, high-density beam scanning enabled the local and dense measurement of the two-dimensional distribution of alternate layers of contraction and relaxation and the propagation of the rapid contraction in the longitudinal direction of LV. These local and minute contractile responses were captured by the local SR measurement but could not be confirmed by velocity measurement.

Similar SR patterns were measured in three consecutive heartbeats for the same subject, although the patterns did not completely correspond. As the local SR reflects the minute change in the local myocardial thickness, subtle changes in

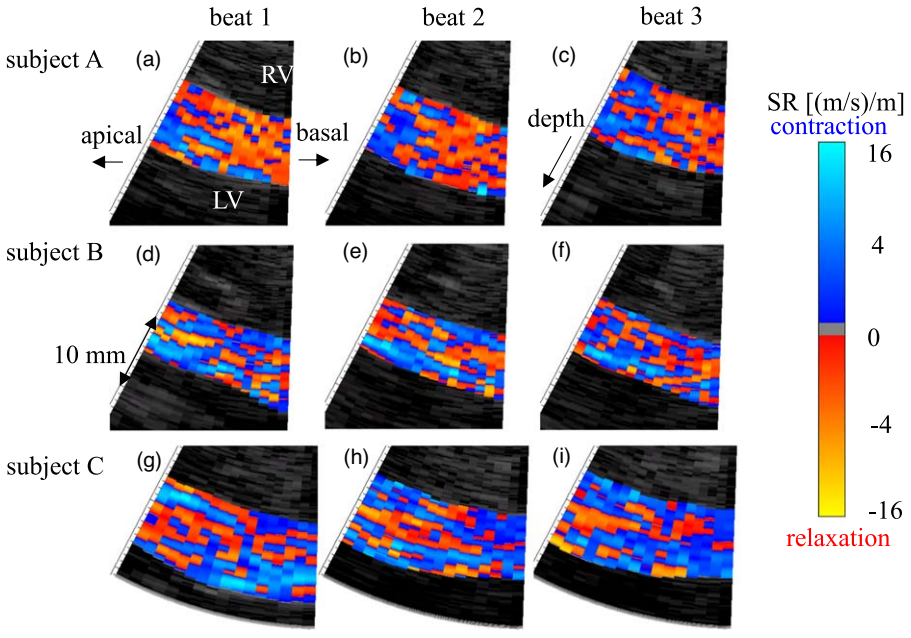

Fig. 3. (Color online) Two-dimensional distributions of SR during the electrocardiogram (ECG) R-wave in three consecutive heartbeats with three subjects.

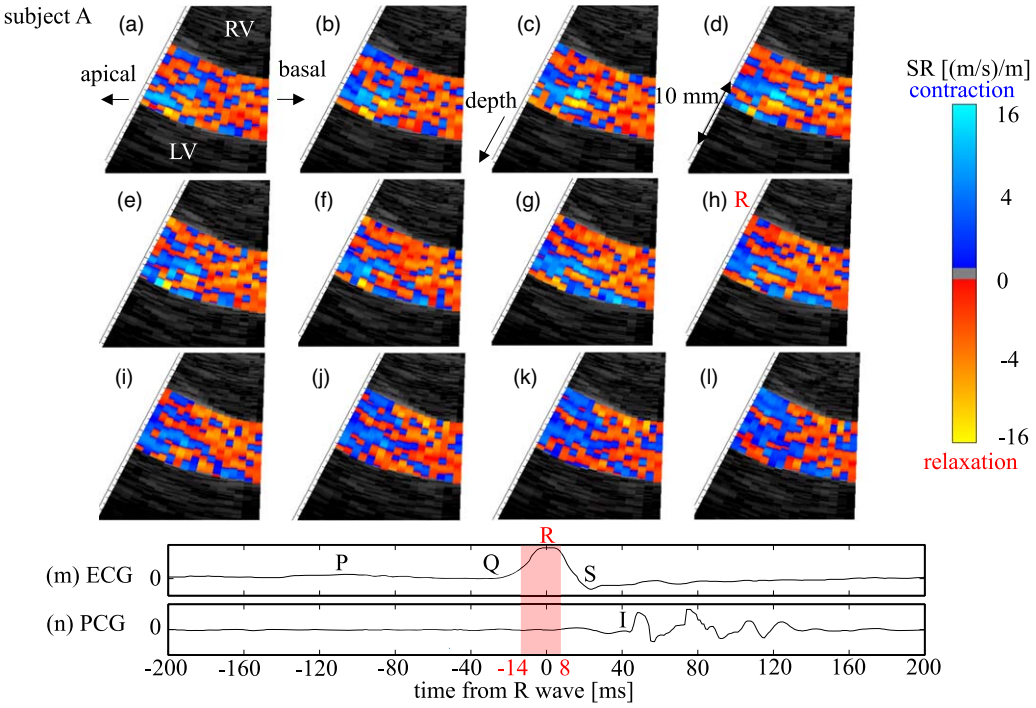

Fig. 4. (Color online) (a)–(l) Two-dimensional distributions of SR around time phase of electrocardiogram (ECG) R-wave every 2 ms for subject A. (m) ECG waveform. (n) Phonocardiogram (PCG) waveform.

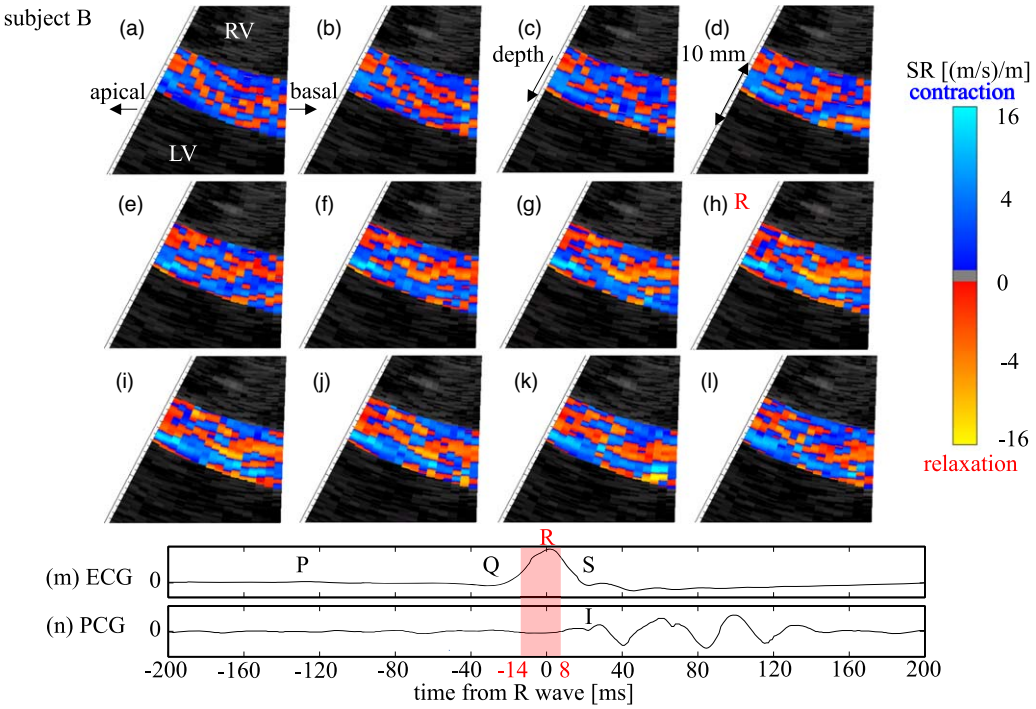

Fig. 5. (Color online) (a)–(l) Two-dimensional distributions of SR around time phase of electrocardiogram (ECG) R-wave every 2 ms for subject B. (m) ECG waveform. (n) Phonocardiogram (PCG) waveform.

the cross-section might affect the local SR measurement in consecutive heartbeats. This effect of the subtle change in the cross-section will be examined in a future study.

4.2. Relationship between alternate layers of contraction and relaxation and physiological mechanism of heart

Let us discuss the relationship between the alternate layers of contraction and relaxation in the two-dimensional distributions of the myocardial SR and the physiological mechanism of the heart. The conducting system in the heart, such as the His-bundle, bundle branch, and Purkinje fiber, allows the electrical excitation to be conducted fast. The myocardial fibers in the IVS are activated by the electrical excitation from the Purkinje fibers connected to the bundle branch. First, in the LV, the apical side of the IVS is activated by the left bundle branch, which runs over the entire surface of the IVS.[21,39] Electrical excitation then occurs in the myocardium. The conduction speed of electrical excitation along the myocardial fiber is 2–4 times faster than that across the myocardial fiber.[40] Thus, the conduction of the electrical

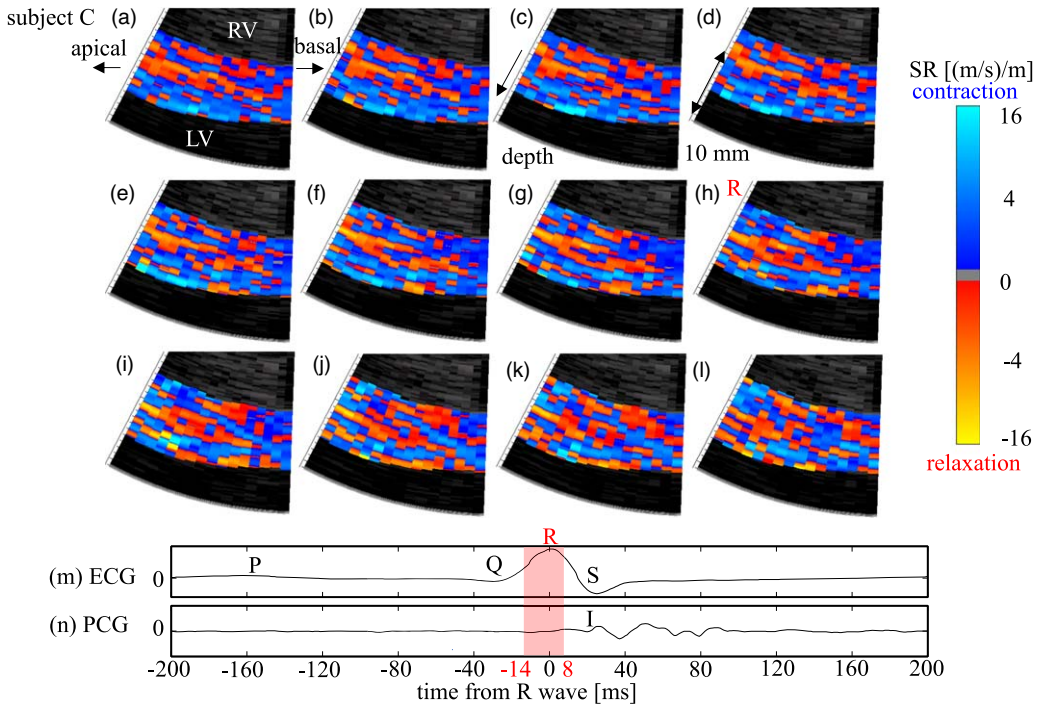

Fig. 6. (Color online) (a)–(l) Two-dimensional distributions of SR around time phase of electrocardiogram (ECG) R-wave every 2 ms for subject C. (m) ECG waveform. (n) Phonocardiogram (PCG) waveform.

excitation depends on the orientation of the myocardial fiber.[41,42] As the LV is constructed with a continuous myocardial band that forms a complex spiral from the basal side to the apical side,[43,44] the heart wall has a layered structure of myocardial sheets in the transmural direction, and the orientation of the myocardial fiber is different in the transmural direction.[18,45,46] Thus, electrical excitation conducts spirally in the LV along the myocardial fibers in each layer.[47]

In the present study, it was confirmed that the contractile response propagated in the longitudinal direction on the LV side of the IVS, which corresponds to the result in the previous study on animal models that the endocardial myocardium contracts earlier than the epicardial myocardium around the time phase of the ECG R-wave.[48] As the direction of the myocardial fiber on the LV side of the IVS is similar to the longitudinal direction,[18,45,46] the propagation of the contractile response in the longitudinal direction indicates that the electrical excitation was conducted along the myocardial fiber direction. Considering the electrical excitation conducts spirally in the LV along the myocardial fibers in each layer, the electrically activated time of the myocardium may be different for each layer in the transmural direction. Thus, the differences in the electrically activated time might have caused the alternate layers of contraction and relaxation, as highlighted by the results of this study.

The mechanism of effective contraction in the layered myocardium was clarified by the alternate layers of contraction and relaxation observed in the local SR distribution. These alternate layers of contraction and relaxation may cause transmural shearing deformation at the boundary between the layers, which occurs due to the layered structure of the myocardial sheets and helps thicken the heart wall effectively.[49,50] In the present study, the alternate layers of contraction and relaxation suggested transmural shearing deformation, which realizes the rapid increase in the internal pressure of the LV in the transition period from diastole to systole.

4.3. Transmitted wave condition for measurement with high-density beam scans and high frame rate

The acquisition area of the RF signals was limited to the part of the IVS to realize the dense and local measurement in the lateral and beam directions with a high frame rate using a focused wave. This measurement condition can be achieved using existing commercial ultrasonic diagnostic apparatuses and can thus be easily applied in clinical applications. However, the acquisition area (24°) was not sufficient to evaluate the entire LV region, as shown in Fig. 1(c) (approximately 90°). Although the propagation of the local and minute contractile response could be measured in the limited acquisition area in the present study, the measurement condition in the present study may not always be optimal.

Alternatively, the parallel beamforming method using a plane wave or a diverging wave may be useful for measuring a larger area densely in the lateral direction.[51–53] These transmitted wave conditions allow us to expand the measurement region with a higher frame rate than that with a focused wave used in the present study. The local SR measurement can also be applied to measurements using a plane wave or diverging wave. However, measurements using a plane wave or diverging wave have a lower spatial resolution and signal-to-noise ratio than those using a focused wave,[54] and the parallel beamforming method requires sufficient computational capacity. Thus, there is a trade-off relationship related to the transmitted wave conditions. Therefore, a suitable transmitted wave condition must be determined by considering the measurement region, spatial and temporal resolution, and feasibility of clinical application in future studies. It is also necessary to clarify the physiological mechanism of the heart to determine a suitable transmitted wave condition.

4.4. Clinical application for evaluating transmurality of myocardial ischemia

Alternate layers of contraction and relaxation were observed in the local SR distribution in healthy subjects. This may have been caused by the conduction of electrical excitation along the myocardial fiber direction. Abnormal conduction of electrical excitation in myocardial ischemia causes a delay in the contractile response,[23,28,29] and the local SR pattern may change owing to the delay of the contractile response. Thus, local SR distribution can visualize the transmurality of myocardial ischemia. The differences in the local SR pattern between healthy subjects and patients will be examined in a future study.

There is a limitation in local SR measurements. As the multifrequency phased-tracking method improves the locality of the SR measurement in the ultrasound beam direction,[37] the ultrasound beam direction corresponds to the transmural direction of the heart wall to realize the local measurement in the transmural direction. Thus, the measurement view is limited, depending on the evaluation. To evaluate the transmurality of myocardial ischemia locally, basal-septal, basal-lateral, mid-septal, and mid-lateral walls can be measured in the parasternal long-axis or short-axis view, apical septal and lateral walls can be measured in the parasternal short-axis view, and the apex can be measured in the apical view. However, the local SR measurement of the anterior and inferior walls may be difficult because the ultrasound beam direction does not correspond to the transmural direction in these measurements. The 17-segment model of the LV is generally used for the assessment of wall motion.[55] It is difficult to evaluate the transmurality of myocardial ischemia using the local SR measurement in the anterior segments (1, 7, and 13) and the inferior segments (4, 10, and 15) in the 17-segment model.

5. Conclusions

The two-dimensional distributions of the myocardial SR, measured with high-density beam scans using our proposed local velocity estimator, exhibited alternate layers of contraction and relaxation around the time phase, representing the onset of the conduction of electrical excitation. The propagation of the local and minute contractile response along the myocardial fiber on the LV side of the IVS was captured for three healthy subjects. The results indicated the effective mechanism of the transition process from diastole to systole, where transmural shearing deformation occurs between the alternate layers of contraction and relaxation. The evaluation of the myocardial SR needs to consider the influence of alternate layers of contraction and relaxation to detect myocardial ischemia in its very early stages by measuring the contractile response caused by electrical excitation. The measurement of myocardial SR, with high-density beam scans, using the multifrequency phased-tracking method, can reveal the effective contraction with transmural shearing deformation and determine the appropriate evaluation index of the contractile function in the layered myocardium.

Acknowledgments

This work was supported in part by JSPS KAKENHI 19K22943.

1) K. A. Reimer, J. E. Lowe, M. M. Rasmussen, and R. B. Jennings, Circulation **56**, 786 (1977).
2) H. Fujiwara, M. Ashraf, S. Sato, and R. W. Millard, Circ. Res. **51**, 683 (1982).
3) H. Kanaide, Y. Taira, and M. Nakamura, Am. J. Physiol. Heart Circ. Physiol. **253**, H240 (1987).
4) R. W. Nesto and G. J. Kowalchuk, Am. J. Cardiol. **57**, C23 (1987).
5) A. E. Stillman et al., Int. J. Cardiovasc. Imaging **34**, 1249 (2018).
6) W. N. McDicken, G. R. Sutherland, C. M. Moran, and L. N. Gordon, Ultrason. Med. Biol. **18**, 651 (1992).
7) H. Kanai, H. Hasegawa, N. Chubachi, Y. Koiwa, and M. Tanaka, IEEE Trans. Ultrason. Ferroelectr. Freq. Control **44**, 752 (1997).
8) A. Heimdal, A. Støylen, H. Torp, and T. Skjærpe, J. Am. Soc. Echocardiogr. **11**, 1013 (1998).
9) J. D'hooge, A. Heimdal, F. Jamal, T. Kukulski, B. Bijnens, F. Rademakers, L. Hatle, P. Suetens, and G. R. Sutherland, Eur. J. Echocardiogr. **1**, 154 (2000).
10) G. R. Sutherland, G. D. Salvo, P. Claus, J. D'hooge, and B. Bijnens, J. Am. Soc. Echocardiogr. **17**, 788 (2004).
11) R. B. Shenouda, I. Bytyçi, M. Sobhy, and M. Y. Henein, Clin. Physiol. Funct. Imaging **40**, 21 (2020).
12) C. Pislaru, M. Belohlavek, R. Y. Bae, T. P. Abraham, J. F. Greenleaf, and J. B. Seward, J. Am. Coll. Cardiol. **37**, 1141 (2001).
13) M. Belohlavek, C. Pislaru, R. Y. Bae, J. F. Greenleaf, and J. B. Seward, J. Am. Soc. Echocardiogr. **14**, 360 (2001).
14) C. Pislaru, P. C. Anagnostopoulos, J. B. Seward, J. F. Greenleaf, and M. Belohlavek, J. Am. Coll. Cardiol. **40**, 1487 (2002).
15) F. Jamal, T. Kukulski, G. R. Sutherland, F. Weidemann, J. D'hooge, B. Bijnens, and G. Derumeaux, J. Am. Soc. Echocardiogr. **15**, 723 (2002).
16) F. Weidemann et al., Circulation **107**, 883 (2003).
17) C. Pislaru, C. J. Bruce, P. C. Anagnostopoulos, J. L. Allen, J. B. Seward, P. A. Pellikka, E. L. Ritman, and J. F. Greenleaf, Circulation **109**, 2905 (2004).
18) P. P. Sengupta, V. K. Krishnamoorthy, J. Korinek, J. Narula, M. A. Vannan, S. J. Lester, J. A. Tajik, J. B. Seward, B. K. Khandheria, and M. Belohlavek, J. Am. Soc. Echocardiogr. **20**, 539 (2007).
19) K. Matre, C. A. Moen, T. Fanneløp, G. O. Dahle, and K. Grong, Eur. J. Echocardiogr. **8**, 420 (2007).
20) R. C. Rimbaş, S. Mihăilă-Baldea, L. Magda, S. I. Vişoiu, D. Muraru, and D. Vinereanu, Ultrason. Med. Biol. **46**, 818 (2020).
21) D. Durrer, R. T. Van Dam, G. E. Freud, M. J. Janse, F. L. Meijler, and R. C. Arzbaecher, Circulation **41**, 899 (1970).
22) H. Kanai, Ultrasound Med. Biol. **35**, 936 (2009).
23) Y. Matsuno, H. Taki, H. Yamamoto, M. Hirano, S. Morosawa, H. Shimokawa, and H. Kanai, Jpn. J. Appl. Phys. **56**, 07JF05 (2017).
24) A. Hayashi, S. Mori, M. Arakawa, and H. Kanai, Jpn. J. Appl. Phys. **58**, SGGE05 (2019).
25) K. F. Kvåle, J. Bersvendsen, E. W. Remme, S. Salles, J. M. Aalen, P. H. Brekke, T. Edvardsen, and E. Samset, IEEE Trans. Med. Imag. **38**, 2665 (2019).
26) M. Pernot, K. Fujikura, S. D. Fung-Kee-Fung, and E. E. Konofagou, Ultrason. Med. Biol. **33**, 1075 (2007).
27) E. E. Konofagou, J. Luo, D. Saluja, D. O. Cervantes, J. Coromilas, and K. Fujikura, Ultrasonics **50**, 208 (2010).
28) J. Provost, W.-N. Lee, K. Fujikura, and E. E. Konofagou, IEEE Trans. Med. Imag. **29**, 625 (2010).
29) J. Grondin, D. Wang, C. S. Grubb, N. Trayanova, and E. E. Konofagou, Comput. Biol. Med. **113**, 103382 (2019).
30) H. Yoshiara, H. Hasegawa, H. Kanai, and M. Tanaka, Jpn. J. Appl. Phys. **46**, 4889 (2007).
31) H. Kanai and M. Tanaka, Jpn. J. Appl. Phys. **50**, 07HA01 (2011).
32) M. Strachinaru, M. L. Geleijnse, N. De Jong, A. Van Den Bosch, M. Michels, A. F. L. Schinkel, A. F. W. Van Der Steen, J. G. Bosch, and H. J. Vos, Ultrason. Med. Biol. **45**, 1987 (2019).
33) H. Kanai, Y. Koiwa, Y. Saito, I. Susukida, and M. Tanaka, Jpn. J. Appl. Phys. **38**, 3403 (1999).
34) M. Tanaka, T. Sakamoto, S. Sugawara, Y. Katahira, H. Tabuchi, H. Nakajima, T. Kurokawa, H. Kanai, H. Hasegawa, and S. Ohtsuki, J. Cardiol. **63**, 313 (2014).
35) M. Tanaka, T. Sakamoto, Y. Katahira, H. Tabuchi, H. Nakajima, T. Kurokawa, H. Kanai, H. Hasegawa, and S. Ohtsuki, J. Cardiol. **64**, 401 (2014).
36) H. Kanai, M. Sato, Y. Koiwa, and N. Chubachi, IEEE Trans. Ultrason. Ferroelectr. Freq. Control **43**, 791 (1996).
37) Y. Obara, S. Mori, M. Arakawa, and H. Kanai, Ultrason. Med. Biol. **47**, 1077 (2021).

38) Y. Obara, S. Mori, M. Arakawa, and H. Kanai, Proc. 41st Symp. on Ultrasonic Electronics, 2020, Vol. 41, p. 3J4.
39) G. K. Massing and T. N. James, Circulation **53**, 609 (1976).
40) T. Sano, N. Takayama, and T. Shimamoto, Circ. Res. **7**, 262 (1959).
41) B. Taccardi, E. Macchi, R. L. Lux, P. R. Ershler, S. Spaggiari, S. Baruffi, and Y. Vyhmeister, Circulation **90**, 3076 (1994).
42) B. B. Punske, B. Taccardi, B. Steadman, P. R. Ershler, A. England, M. L. Valencik, J. A. McDonald, and S. E. Litwin, J. Electrocardiol. **38**, 40 (2005).
43) F. Torrent-Guasp, M. Ballester, G. D. Buckberg, F. Carreras, A. Flotats, I. Carrió, A. Ferreira, L. E. Samuels, and J. Narula, J. Thorac. Cardiovasc. Surg. **122**, 389 (2001).
44) F. Torrent-Guasp, M. J. Kocica, A. Corno, M. Komeda, J. Cox, A. Flotats, M. Ballester-Rodes, and F. Carreras-Costa, Eur. J. Cardio-Thoracic Surg. **25**, 376 (2004).
45) R. A. Greenbaum, S. Y. Ho, D. G. Gibson, A. E. Becker, and R. H. Anderson, Heart **45**, 248 (1981).
46) J. Chen, W. Liu, H. Zhang, L. Lacy, X. Yang, S.-K. Song, S. A. Wickline, and X. Yu, Am. J. Physiol. Heart Circ. Physiol. **289**, H1898 (2005).
47) H. C. Coghlan, A. R. Coghlan, G. D. Buckberg, M. Gharib, and J. L. Cox, Semin. Thorac. Cardiovasc. Surg. **13**, 333 (2001).
48) H. Ashikaga, B. A. Coppola, B. Hopenfeld, E. S. Leifer, E. R. McVeigh, and J. H. Omens, J. Am. Coll. Cardiol. **49**, 909 (2007).
49) I. J. LeGrice, Y. Takayama, and J. W. Covell, Circ. Res. **77**, 182 (1995).
50) K. D. Costa, Y. Takayama, A. D. McCulloch, and J. W. Covell, Am. J. Physiol. Heart Circ. Physiol. **25**, H595 (1999).
51) H. Hasegawa and H. Kanai, J. Med. Ultrasonics **38**, 129 (2011).
52) H. Hasegawa and H. Kanai, IEEE Trans. Ultrason. Ferroelectr. Freq. Control **61**, 1779 (2014).
53) S. Nunome, R. Nagaoka, and H. Hasegawa, Jpn. J. Appl. Phys. **59**, SKKE01 (2020).
54) N. Furusawa, S. Mori, M. Arakawa, and H. Kanai, Jpn. J. Appl. Phys. **58**, SGGA08 (2019).
55) M. D. Cerqueira, N. J. Weissman, V. Dilsizian, A. K. Jacobs, S. Kaul, W. K. Laskey, D. J. Pennell, J. A. Rumberger, T. Ryan, and M. S. Verani, Circulation **105**, 539 (2002).